Computational de Novo Design and Characterization of a Protein That Selectively Binds a Highly Hyperpolarizable Abiological Chromophore

H. Christopher Fry,[‡] Andreas Lehmann,[‡,¶] Louise E. Sinks,[‡] Inge Asselberghs,[⊥] Andrey Tronin,[‡] Venkata Krishnan,[‡] J. Kent Blasie,[‡] Koen Clays,[⊥] William F. DeGrado,*,[∇] Jeffery G. Saven,*,[‡] and Michael J. Therien*,[§]

[‡]Department of Chemistry, University of Pennsylvania, Philadelphia, Pennsylvania 19104-6323, United States
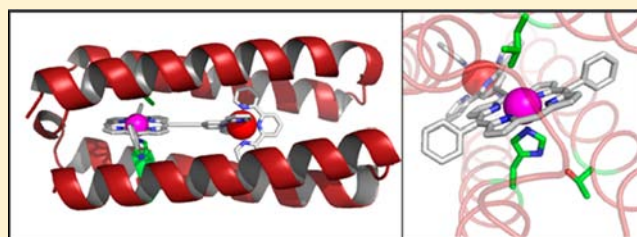
[⊥]Department of Chemistry, University of Leuven, B-3001 Leuven, Belgium

[∇]Department of Pharmaceutical Chemistry, Investigator, Cardiovascular Research Institute, University of California at San Francisco, San Francisco, California 94158-9001, United States

[§]Department of Chemistry, Duke University, Durham, North Carolina 27708-0354, United States

Ⓢ Supporting Information

ABSTRACT: This work reports the first example of a single-chain protein computationally designed to contain four α-helical segments and fold to form a four-helix bundle encapsulating a supramolecular abiological chromophore that possesses exceptional nonlinear optical properties. The 109-residue protein, designated **SCRPZ-1**, binds and disperses an insoluble hyperpolarizable chromophore, ruthenium(II) [5-(4′-ethynyl-(2,2′;6′,2″-terpyridinyl))-10,20-bis(phenyl)-porphinato]zinc(II)-(2,2′;6′,2″-terpyridine)$^{2+}$ (**RuPZn**) in

aqueous buffer solution at a 1:1 stoichiometry. A 1:1 binding stoichiometry of the holoprotein is supported by electronic absorption and circular dichroism spectra, as well as equilibrium analytical ultracentrifugation and size exclusion chromatography. **SCRPZ-1** readily dimerizes at micromolar concentrations, and an empirical redesign of the protein exterior produced a stable monomeric protein, **SCRPZ-2**, that also displayed a 1:1 protein:cofactor stoichiometry. For both proteins in aqueous buffer, the encapsulated cofactor displays photophysical properties resembling those exhibited by the dilute **RuPZn** cofactor in organic solvent: femtosecond, nanosecond, and microsecond time scale pump−probe transient absorption spectroscopic data evince intensely absorbing holoprotein excited states having large spectral bandwidth that penetrate deep in the near-infrared energy regime; the holoprotein electronically excited triplet state exhibits a microsecond time scale lifetime characteristic of the **RuPZn** chromophore. Hyper-Rayleigh light scattering measurements carried out at an incident irradiation wavelength of 1340 nm for these holoproteins demonstrate an exceptional dynamic hyperpolarizabilty ($\beta_{1340} = 3100 \times 10^{-30}$ esu). X-ray reflectivity measurements establish that this de novo-designed hyperpolarizable protein can be covalently attached with high surface density to a silicon surface without loss of the cofactor, indicating that these assemblies provide a new approach to bioinspired materials that have unique electro-optic functionality.

INTRODUCTION

Natural cofactors confer function to biological proteins that cannot be achieved with the amino acids alone. Examples of such functions include transduction of light energy, oxygen binding, and enzymatic catalysis. Natural cofactors include metal atoms, metal clusters, flavins, quinones, and metal-loporphyrins. Synthetic proteins provide the potential to incorporate nonbiological cofactors that can confer new functionalities not seen in nature. For many cofactor-binding proteins, non-covalent interactions play a critical role in positioning the cofactor within the protein matrix. Computational protein design engineers these noncovalent interactions, and can now create systems capable of incorporating synthetic nonbiological cofactors, thereby yielding peptide-based systems

with novel functionalities.[1−5] Importantly, the interior of the designed protein scaffold can be used to control cofactor conformation, solubility, location, and orientation, as well as the cofactor local molecular and dielectric environment, thus providing multiple mechanisms by which to modulate cofactor properties; likewise, design modifications of the protein exterior facilitate the nature of their organization with identical and dissimilar proteins, and target their placement at surfaces and interfaces. To realize protein complexes that possess novel functions through specific binding of large non-natural cofactors, computational protein design is critical.

Chromophores that feature extended π-electron systems and electronic asymmetry can exhibit exceptionally large molecular hyperpolarizabilities;[6–22] incorporation of such an abiological cofactor into a de novo-designed protein provides a strategy to define a protein having unique electro-optic function. Dipolar, "push–pull" chromophores that have desirable nonlinear optical (NLO) functionality often exploit a conjugated bridge to couple integral donor and acceptor elements. One striking example is ruthenium(II) [5-(4′-ethynyl-(2,2′;6′,2″-terpyridin-yl))-10,20-bis(phenyl)porphinato]zinc(II)-(2,2′;6′,2″-terpyri-dine)²⁺ (**RuPZn**, Chart 1),[13,14] a hyperpolarizable super-

Chart 1
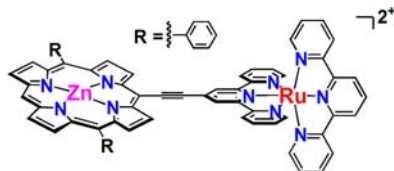
molecular chromophore that features highly conjugated (porphinato)metal and poly(pyridyl)metal components. In **RuPZn** and related supermolecules, (porphinato)zinc $\pi-\pi^*$- and metal polypyridyl-based charge-resonance absorption oscillator strength are extensively mixed, and the respective charge transfer transition dipoles of these building blocks are aligned along the highly conjugated molecular axis. These structures manifest significant inter-pigment electronic inter-actions, display unusual dependences of the sign and magnitude of the hyperpolarizability upon incident irradiation frequency, and exhibit extraordinarily large dynamic hyperpolarizability (β_λ) values at long wavelengths (1.3–1.55 μm).[13,14,18–20,23–26] **RuPZn**, for example, possesses an exceptional β_λ value at an incident irradiation wavelength of 1300 nm (β_{1300} = 5100 × 10^{-30} esu).[13]

The development of macroscopic materials that possess impressive nonlinear properties based on these chromophores requires control and ordering of hyperpolarizable molecules in a non-centrosymmetric arrangement throughout the medium. For dipolar molecules dispersed randomly within the solid state, ground-state electrostatic interactions drive detrimental, centrosymmetric aggregation that diminishes the macroscopic electro-optic response. Although experimental strategies exist that minimize the magnitude of antiparallel dipole–dipole interactions of NLO chromophores in the condensed phase, such as electric-field poling of chromophoric guests within polymeric hosts, it is important to underscore that the net bulk-phase dipolar order realized in such NLO materials rarely, if ever, exceeds a level beyond that of several percent of the chromophoric dopants present in the medium.[27–34]

As proteins bind and control the conformation and orientation of cofactors, modulate their functional properties, and encode for protein–protein organization over mesoscopic and macroscopic length scales, de novo proteins offer new opportunities to control NLO functional elements. In this report, we demonstrate (i) that computational protein design can be utilized to realize a single-chain protein with four α-helical segments that folds to bind and encapsulate the supermolecular **RuPZn** chromophore, (ii) that this de novo protein manifests photophysical and electro-optical properties characteristic of its **RuPZn** cofactor, and (iii) that a variant of this protein having appropriate C-terminal functionality

provides a self-assembled, ordered monolayer of this novel functional protein−cofactor complex on silicon at high-density surface coverage, while preserving its classic NLO response. Taken together, these results illustrate a practicable approach toward designing protein-based electro-optic devices.

■ METHODS

Computational Design of Protein Structure. The single-chain four-helix bundle protein was designed using previously described computationally guided methods for backbone construction, loop selection, and side-chain placement.[1,3,4] A tetrameric helix bundle backbone was constructed to accommodate the cofactor and contained a hydrogen-bonded His-Thr pair, where the His axially coordinates the central Zn(II) ion of the porphyrin macrocycle (Figure 1).[4] Bundle
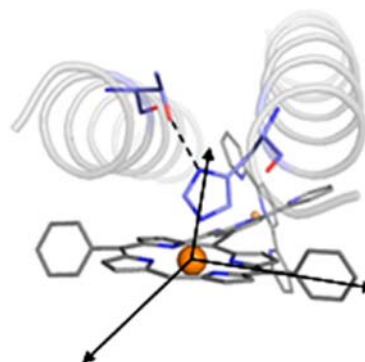

Figure 1. Helix bundle construction: orientation of coordinating fixed histidine and stabilizing threonine with respect to the porphyrin macrocycle.
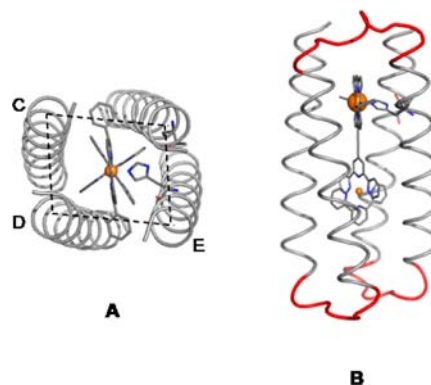

Figure 2. Four-helix bundle backbone after backbone construction, top view (A), and introduction of loops, side view (B). The interhelical distances depend on the position of the helices with respect to the porphyrin macrocycle: helices on one side of the PZn unit (*cis*-porphyrin) are closer than helices on opposite sides (*trans*-porphyrin). That is, the *cis*-porphyrin distance CD in panel A is smaller than the *trans*-porphyrin distance DE.

construction resulted in a tetramer of antiparallel 24-residue α-helices (Figure 2A). Loops connecting these helices were selected from a database of natural α-helical protein structures and were spliced so as to not conflict sterically with the remainder of the structure (Figure 2B).[1] The loops were positioned so as to minimize root-mean-square difference (rmsd) between the respective C_α atoms of the loop termini and the C_α atoms of the helix termini (Figure 2).[1] Within the resulting 109-residue structure, residues were relaxed via energy minimization using CHARMM[35] and the steepest decent method for 15 steps. Bond lengths and angles were checked using PROCHECK.[36] As discussed in previous work,[1,3,4] the cofactor was positioned so as to achieve axial Zn(II) coordination via the predetermined His residue, and the
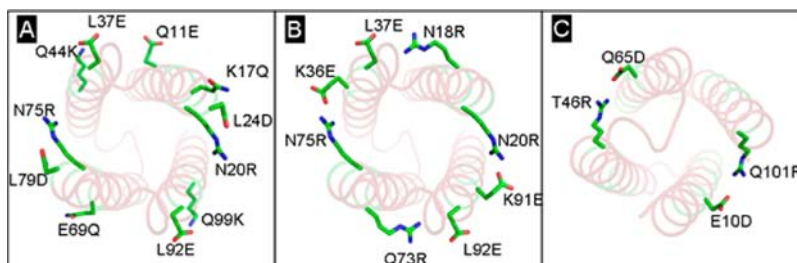
Figure 3. Empirical redesign to yield **SCRPZ-2**: (A) the 11 residues adopted from **PA$_{SC}$**, (B) salt-bridge pairs, and (C) salt-bridge pairs across the hydrophobic patch.

internal torsion about the ethyne bridge was selected so that the angle between the planes of the porphyrin and the bridged terpyridyl moiety is commensurate with the superhelical twist of the four-helix bundle.

Protein Design: Sequence SCRPZ-1. Computational methods guided the selection of the protein sequence. In the design calculations, the tertiary structure and presence of the **RuPZn** cofactor are present as described above. In addition, the residues involved in Zn(II) coordination of the cofactor, His45 and its hydrogen-bonded partner Thr8, were constrained to have these identities as well as side-chain conformations consistent with Zn(II) coordination.[1,3,4] A statistically guided, computationally assisted design strategy was applied that utilizes a self-consistent approach to estimate site-specific probabilities of the amino acids at variable positions as discussed previously.[1,4] Protein design was carried out in two rounds of computational design calculations.[2,37]

In the first calculation, all amino acids were allowed at the 106 variable positions except for Cys, His, and Pro. Cys and His were precluded to prevent untargeted Zn(II) coordination and disulfide formation; Pro, a known helix breaker, was allowed only in the loop regions at residues where it is present in the template loops. The residue identities were selected to be the most probable amino acids whose probability p_1 satisfies $p_1 \geq 0.3$: LEU2, GLY9, ILE12, ALA16, VAL19, GLU21, LEU31, LEU34, ALA38, ALA49, ASN56, GLU57, GLN63, GLY64, ILE67, ALA71, VAL74, LEU78, GLU82, LEU86, ALA93, LEU103, and LYS107. (Numbering of residues is chosen such that the first residue is denoted MET0, which was appended to the N-terminus of the designed sequence.) Many of these positions are within the interior of the protein structure. Residues in the loop regions are solvent exposed and multiple amino acids are probable at most positions. Positions 26 and 81 adopt an alpha-left configuration, and these were specified to be Gly (GLY26, GLY81), which is consistent with the Schellman α_L-β turn of these loop regions.[38] Previous studies of turns near α-helices also identified a preference for Asp at positions 29 and 84 in these turns: ASP29 and ASP84.[38] Residue 27 has a structure similar to that of GLU82, and its identity was specified as GLU27. The following residues were constrained to have the identities present in the template loops, identities that are also among the probable amino acids at each site: SER30, LEU48, TYR50, ASN51, ARG52, MET53, GLY54, ALA55, THR58, ALU59, GLY81, ASP84, and SER85.

After fixing the identities discussed above, the probabilities of the amino acids at the remaining positions were determined using a second calculation. The following are the most probable amino acid identities in their respective positions: GLU1, GLU3, LYS4, LEU5, ARG6, GLN7, GLU10, GLN11, GLN14, ILE15, LYS17, GLN18, ILE22, MET23, LYS25, GLU32, LEU35, LYS36, TYR39, ILE42, GLN44, GLN47, ILE60, LYS62, GLN66, GLU69, GLN73, ASN75, GLU76, LYS80, GLU87, GLN88, ILE90, LYS91, ILE97, GLN99, GLN101, GLU102, GLU105, LYS106, and ASN108. Probable hydrophobic amino acids were selected at residues near the cofactor or at helix−helix interfaces: LEU13, LEU37, LEU41, ALA56, MET61, LEU68, ILE70, VAL77, LEU89, LEU92, LEU96, LEU100, and PHE104. Positions 27 and 82 were specified as the probable ASP (ASP27, ASP82), and previous work suggests a large propensity for the amino acid at this position in the turn.[38] Positions 24 and 79 were specified as LEU, the identity in the template loop, which is among the

probable amino acids (LEU24, LEU79). The following amino acids were selected from among the probable amino acids to foster potential hydrogen bonding and salt-bridge interactions observed in the modeled protein: GLN33, GLU40, GLN43, THR47, GLU53, GLU54, ASP57, GLN65, GLN72, LYS83, TYR94, GLN95, and GLN98. Due to its proximity to the cofactor, a small hydrophobic amino acid was selected from among the probable amino acids at position 56: ALA56. The resulting protein is denoted **SCRPZ-1**: MELEKLRQTG EQILQIAKQV NEIMLKGDDD SLEQLIKLAY ELIQQHTQLA YNRQEAADTE IMKQGQQILE IAQQVNEVLL KGDKDSLEQL LKLAYQLIQQ LQELFEKKN.

Empirical Redesign: Sequence SCRPZ-2. To explore control of oligomerization state in the absence of co-solvents and the robustness of the folding and binding properties of the protein with respect to mutation, we chose to redesign the protein exterior. **SCRPZ-1** has a neutral charge and exterior hydrophobic patches (Figure S2). Using the **SCRPZ-1** structure and sequence, the exterior of the protein was redesigned with the intent of increasing the number of ionizable residues on the protein exterior, while incorporating interhelical salt bridges to ensure bundle stability. The model structure of **SCRPZ-1** was aligned with a similarly designed protein, **PA$_{SC}$**, a 109-residue protein that is a monomer under similar conditions (Figure S1).[1] For this alignment, ten sequential residues beginning 5 residues away from the $\alpha_I\beta$ (GD) turn from each helix were selected. Overall, 40 residues were aligned and found to have a 1.33 Å rmsd (Figure S1). Eleven exterior residues were mutated to the corresponding exterior amino acid in **PA$_{SC}$**: Q11E, K17Q, N20R, L24D, L37E, Q44K, E69Q, N75R, L79D, L92E, and Q99K (Figure 3A). Two other positions, L24 and L79 appeared in the loop template and were modified to charged residues consistent with the **PA$_{SC}$** design. Upon inspection of the structure, N20R, L37E, N75R, and L92E appeared to be good candidates from which to engineer salt-bridged pairs: N20R-K91E, L37E-N18R, N75R-K36E, and L92E-Q73R (Figure 3B). The following modifications were made to generate ionic pairs spanning a hydrophobic patch that resulted from complementary cofactor and interhelical, hydrophobic packing of **SCRPZ-1**: E10D-Q101R and T46R-Q65D (Figure 3C). The resulting protein, **SCRPZ-2**, possesses 19 mutations relative to **SCRPZ-1**. The redesigned protein presents a more charged exterior, as well as interhelical salt bridges that span a hydrophobic patch (Figure S2). The resulting protein is denoted **SCRPZ-2**: MELEKLRQTG DEILQIAQRV REIMDKGDDD SLEQL-LEEAY ELIQKHRQLA YNRQEAADTE IMKQGDQILQ IAQRV-REVLD KGDKDSLEQL IEEAYQLIQK LRELFEKKN.

SCRPZ-1, SCRPZ-2, and SCRPZ-3 Gene Construction and Expression. Each synthetic gene (DNA 2.0 for **SCRPZ-1** and Genscript for **SCRPZ-2**) were preceded by the *Nde*I and terminated by the *Hind*III restriction sites and codon optimized for expression in *E. coli*. The genes were successfully ligated to the *Nde*I/*Hind*III-digested pET24a+ expression vector (which contains the IPTG-inducible T7 promoter) using T4 ligase following the manual protocol. Gene amplification with *pfu* polymerase was performed using standard T7 promoter and T7 terminator DNA primers and sequencing of the amplified product allowed the identification of the successfully ligated gene into the pET24a+ expression vector (University of Pennsylvania sequencing center). See Supporting Information (SI) for the gene sequences used to express the proteins **SCRPZ-1** and **SCRPZ-2**.

The synthetic gene designed to express a C-terminus (Gly)$_3$Cys sequence to enable surface immobilization via coupling chemistry was constructed via PCR amplification utilizing *taq* polymerase and the following primers: (*SCRPZ_3 Promoter*) GCAG *CAT ATG* GAA CTG GAA AAA CTG CGT CA and (*SCRPZ_3 Terminator*) GCAG *AAG CTT* TTA ACA TCC GCC TCC GTT TTT CTT TTC GAA CA. The resulting product was then double digested using the *Nde*I and *Hin*dIII restriction enzymes in order to remove the nonsense GCAG sequence. Agarose gel electrophoresis was used to purify the digested gene insert. The gene was then inserted into the pET 24a$^+$ expression vector followed by gene amplification and sequencing to confirm insertion as described previously. See SI for the gene sequence that expresses the protein **SCRPZ-3:** MELEKLRQTG EQILQIAKQV NEIMLKGDDD SLEQLIKLAY ELIQQHTQLA YNRQEAADTE IMKQGQQILE IAQQVNEVLL KGDKDSLEQL LKLAYQLIQQ LQELFEKKN GGGC.

The proteins were expressed using BL21(DE3) cells. The cells were grown to an optical density at 600 nm between 0.6 and 0.9 prior to induction with 1 mM IPTG. After 3 h, the cells were centrifuged (20 min, 4000g, 4 °C), and the LB supernatant was decanted. The resulting pellet was resuspended in DPBS (30 mL), and the cells were lysed by sonication. Following centrifugation (30 min, 15000g, 4 °C), the supernatant was heat-denatured at 70 °C, followed by another centrifugation (30 min, 15000g, 4 °C). The protein remained in the supernatant, as visualized by gel electrophoresis (MES SDS−PAGE), and was lyophilized. The crude material obtained from the expression was reconstituted in Millipore purified water at a concentration of 6 mg/mL for purification by reversed phase HPLC (Varian ProStar) over a C4 column (Vydac). Collection of the major peak and analysis by MALDI-TOF MS (PerSeptive Biosystems Voyager DE) indicated correct mass spectral data (**SCRPZ-1** calcd 12708.5, found, 12710.0; **SCRPZ-2** calcd, 12943.6, found, 12944.0; **SCRPZ-3** calcd, 12982.8, found, 12983.2). Once the protein was purified and thoroughly lyophilized, it was reconstituted in buffer (50 mM phosphate, 150 mM NaCl, pH 7.5), typically to a concentration of 200−300 μM, and used immediately.

Cofactor "Reconstitution": Holoprotein Preparation. Samples were prepared by diluting a concentrated stock solution into 50 mM phosphate buffer with 150 mM sodium chloride at pH 7.5. A 2-fold excess of the cofactor **RuPZn** (see SI for synthetic scheme)^{13} was added from a 5 mM DMSO stock solution (note: final DMSO concentration in buffer was kept below 1%). The sample was heated to >50 °C for 15 min, followed by cooling to room temperature. Any unbound cofactor would visibly aggregate and was removed via spin filtration (Millipore Ultrafree MC 0.22 μm). To remove DMSO, chromatography with a NAP5 or PD10 (GE Healthcare) gravity column equilibrated with the desired buffer as eluent was sufficient. Amicon centrifugal devices were used when necessary to concentrate the prepurified samples to desired concentrations. Samples were made typically at **RuPZn** concentrations ranging from 25 to 100 μM.

Electronic Absorption and Circular Dichroism Spectroscopy. Electronic absorption spectral data were obtained on a Hewlett-Packard 8453 spectrophotometer at room temperature in a 1 cm quartz cuvette. To evaluate the secondary structure and stability of the protein and the complex, CD spectroscopy was carried out at 25 °C on a Jasco 810 spectropolarimeter in 0.1 cm cuvettes. Buffer conditions for CD experiments were 50 mM phosphate buffer, 150 mM sodium chloride, pH 7.5; the protein concentration was 25−50 μM. Samples were prepurified with either NAP5 or PD10 gravity columns to remove excess cofactor and DMSO, as the organic solvent absorbs light in the 190−260 nm scanning region of the spectrum. For thermal denaturation experiments, the ellipticity at 222 nm was monitored as a function of temperature. Data were collected every 2 °C with a heating rate of 1 °C/min followed by a 4 min equilibration time.

To determine the peptide:cofactor stoichiometry, titration experiments were performed. First, 300 μL of a solution of 17.5 μM **RuPZn** was prepared in 50 mM phosphate buffer, containing 150 mM sodium chloride, pH 7.5, and 1% (w/v) octylglucopyranoside (OG). (The surfactant OG is necessary for cofactor solubilization.) Next, 2.0 μL aliquots of 320 μM **SCRPZ-1** were introduced into the solution and

allowed to equilibrate for 5 min before each spectrum was obtained. **RuPZn** binding was monitored spectrophotometrically at 660 nm as the protein was titrated into the cofactor solution. A similar procedure using the same buffer conditions was followed for analyzing **SCRPZ-2** binding: to 300 μL of 8 μM **RuPZn** were added 2.0 μL aliquots of 113 μM **SCRPZ-2.**

Size Exclusion Chromatography. Gel filtration profiles were obtained using a Superdex 75 10/300GL column on an FPLC system (GE Healthcare AKTA FPLC system). To evaluate the oligomeric state, 100 μL of a 20 μM sample was injected onto the column and eluted with a 50 mM phosphate buffer, 150 mM NaCl, pH 7.5 mobile phase at a flow rate of 0.5 mL/min. In cases where aggregation was suspected, 5% isopropanol was added to the elution buffer in an attempt to break up aggregates. The approximate molecular weight (MW$_{app}$) was calculated from a standard curve obtained using the mass standard blue dextran, V_e (void volume): aprotinin, 6500 Da; cytochrome *c*, 12 400 Da; carbonic anhydrase, 29 000 Da; and albumin, 66 000 Da.

Analytical Ultracentrifugation: Sedimentation Equilibrium. For analytical ultracentrifugation (AU), 125 μL samples of 160 μM apoprotein and 20 μM holo-protein in 50 mM phosphate buffer and 150 mM NaCl at pH 7.5 were prepared. The samples were filtered prior to analysis using a 0.22 μm spin filter. Analysis was performed at 25 °C using a Beckman XL-I analytical ultracentrifuge. The absorbance was monitored at 280 nm for apo-protein and 430 nm for holo-protein, and the samples were centrifuged at 20 000, 25 000, and 30 000 rpm. The data were analyzed using a modified global fitting routine in IGOR Pro (Wavemetric) and assumed a single molecular weight species. The protein maintains its calculated partial specific volume when the monomeric molecular weight is held constant. The partial specific volume (ν) of 0.735 mL/g and solvent density (ρ) of 1.01 g/mL were calculated using SEDNTERP.

Pump−Probe Transient Absorption Spectroscopy. Nano-second transient absorption spectra were recorded with a previously described Q-switched Nd:YAG laser system (DCR-1A, Quanta Ray, Mountain View, CA).^{39} Samples were prepared at concentrations of 10 μM in 50 mM phosphate 150 mM NaCl buffer at pH 7.5 followed by three freeze (−40 °C)/ pump/thaw cycles in a 1 cm quartz cuvette. The monoexponential triplet-state lifetime data were analyzed using a single exponential decay model in the program Origin 7.5.

Picosecond transient absorption spectra were acquired using standard pump−probe methods. A schematic of this transient optical system, as well as a detailed description of the apparatus, have been described previously.^{14} Probe light was generated using an all-reflective optics configuration. Polarization of the pump beam was set at the magic angle by a Rochon polarizer; polarization of the probe light was set using a waveplate and a rotating sapphire plate to obtain horizontal polarization. The polarization of the probe beam was confirmed using crossed polarizers. All these experiments utilized 1 mm path length fused-silica sample cells. Samples were all prepared between 75 and 125 μM in 50 mM phosphate, 150 mM NaCl buffer at pH 7.5. The samples were deoxygenated via three consecutive freeze (−5 or −40 °C)/pump/thaw cycles or a 30 min argon purge. All transient spectra reported represent averages obtained over at least three scans, with each scan consisting of 150−250 time points.

Hyper-Rayleigh Light Scattering Measurements. Femto-second hyper-Rayleigh light scattering (HRS) experiments were performed at 800, 1300, and 1340 nm.^{40,41} Disperse red 1 (DR1; $\beta_{1300} = 54 \times 10^{-30}$ esu; $\beta_{1340} = 50 \times 10^{-30}$ esu)^{41} in CHCl$_3$ was utilized as a reference chromophore. For these external references in different solvents, standard local field correction factors were applied $[((n_D^2 + 2)/3)^3$, where n is the refractive index of the solvent (chloroform, 1.4459; water, 1.333) at the sodium D line]. Note that these experiments were performed at low (μM) holoprotein (chromophore) concentrations where the linearity of the HRS signal as a function of protein (chromophore) concentration confirmed that no significant self-absorption of the SHG signal occurred in these experiments. For HRS experiments carried out at an irradiation wavelength of 800 nm, crystal violet (CV) in methanol solvent was utilized as a chromophoric reference ($\beta_{800} = 338 \times 10^{-30}$ esu). Note that in these experiments, the

difference in molecular symmetry (octopolar for CV, dipolar for **RuPZn**) has been taken into account.[40] The samples were prepared as described above. To ensure that the observed HRS signal at the second-harmonic wavelength is purely second-order scattering, and not due to multiphoton fluorescence, frequency-resolved femtosecond HRS experiments were performed. These measurements show neither a demodulation nor an increase in phase delay with increasing amplitude modulation, indicating the absence of any multiphoton fluorescence contribution to the observed HRS signals. This finding is in line with the results reported earlier for other members of this class of (polypyridyl)ruthenium−(porphinato)zinc(II) chromophores.[13,26]

SCRPZ-3 Immobilization on Silicon Substrates. The reducing agent, 1,4-dithiothreitol (DTT) was purchased from Acros Organics (Morris Plains, NJ). The silane used for alkylation, 3-amino-propyldimethylethoxysilane, was obtained from Gelest Inc. (Morris-ville, PA). The linker, succinimidyl 4-[N-maleidomethyl]-cyclohexane-1-carboxylate (SMCC), as well as other solvents and reagents used for self-assembly, were obtained from Fisher Scientific (Springfield, NJ). All purchased chemicals were used without further purification. The fused silica slides (UV grade; 25 mm × 70 mm) were bought from Esco Products (Oak Ridge, NJ) and the 3-in.-diameter silicon wafers (n-type Si:P, 600 μm thick) were purchased from El-Cat Inc. (Waldwick, NJ). In order to increase the sensitivity and spatial resolution of the X-ray reflectivity (XR) technique by employing an interferometric approach, multilayers comprised of 50 Å Si−20 Å Ge−20 Å Si−20 Å Ge−20 Å Si were deposited sequentially onto the silicon wafers via magnetron sputtering. This fabrication was performed in the deposition laboratory at the Advanced Photon Source at Argonne National Laboratory (Argonne, IL).

The silicon wafers with the multilayer structure were cut into pieces of 20 mm × 10 mm dimension suitable for X-ray experiments, while the fused silica slides were cut into pieces of 25 mm × 35 mm dimension suitable for linear UV/visible absorption spectroscopy. Both the silicon wafer slides and fused silica slides were treated together, from cleaning through monolayer deposition. The slides were cleaned using methanol, chloroform, and acetone through sonication in each of these solvents for 10 min. Later the slides were alkylated with 3-aminopropyldimethylethoxysilane under an Ar atmosphere by immersing the substrates in a 5% silane solution in toluene for 1 h. The slides were rinsed with toluene and sonicated in this solvent for 10 min. The slides were cured subsequently under Ar at 67 °C for 1 h. For linker attachment, the slides were placed in 1 mM SMCC solution in anhydrous methanol for 1 h, following which they were rinsed with methanol, sonicated for 10 min, and dried using a jet of Ar gas.

SCRPZ-3 possesses a C-terminal cysteine to facilitate the covalent attachment of the peptide bundle to a suitably alkylated surface of an inorganic substrate. **SCRPZ-3** incorporating the **RuPZn** chromophore was first treated with DTT in 1:1 mol ratio, for 10 min at room temperature, to remove possible disulfide linked peptides. Subsequent dialysis against potassium phosphate buffer (100 mM at pH 7) for 3 h at room temperature was employed to remove DTT from the protein solution. For covalent attachment, slides possessing the SMCC linker on their surface were incubated in a **SCRPZ-3** solution (50 μM protein in 100 mM potassium phosphate buffer at pH 8) at 4 °C overnight to allow covalent bond formation between the SMCC linker and the C-terminal cysteine. The protein-monolayer-functionalized substrates were then washed several times with flowing ultrapure water (Millipore, Billerica, MA) in order to remove nonspecifically adsorbed molecules. The substrates were then stored under Ar at 4 °C prior to experimental measurements.

X-ray Reflectivity and Linear Electronic Absorption Spectroscopy. The X-ray reflectivity (XR) data for the covalently attached monolayer films on silicon substrates having a multilayer structure were collected using a triple-axis diffractometer with an Enraf-Nonius F-591 rotating-anode X-ray source and a scintillation detector. A curved LiF crystal was utilized to select and collimate the Cu Kα_1 spectral line. Further collimation was achieved by the slits before and after the specimen chamber, with the resolution determined by the analyzer crystal before the scintillation detector. Reflectivity data were

recorded over the range of photon momentum transfer Q_z from 0.01 to 0.52 Å^{-1}. At lower incident angles, the X-ray beam was attenuated by nickel foils inserted upstream from the specimen. The specimen chamber with Kapton windows was maintained at 24 °C. A LI-610 dewpoint generator (LI-COR, Lincoln, NE) was additionally fitted to maintain the relative humidity inside the chamber in excess of 96% in helium. Linear electronic absorption spectroscopic (EAS) data were collected at room temperature from the self-assembled monolayer films on fused silica substrates using a Lambda 650 spectrophotometer (Perkin Elmer, Waltham, MA).

The raw XR data from the covalently attached monolayer films were normalized by the Fresnel function, using the software C-Plot (Certified Scientific Software, Cambridge, MA), to eliminate the effects due to dynamical scattering from a single ideal interface, leaving the kinematical scattering due to the presence of the multilayer reference structure with the attached self-assembled monolayer on its surface. Subsequent analysis was performed using the Distorted Wave Born Approximation and the so-called box refinement algorithm,[42] implemented via Mathematica 4.2 (Wolfram Research, Champaign, IL), for solving the phase problem and obtaining the electron-density profile that fully accounts for the observed reflectivity data. This approach has been thoroughly described in prior publications[43,44] for covalently attached monolayer films on multilayer reference structures. The linear EAS data were used to confirm that the **RuPZn** chromophore remained bound to the **SCRPZ-3** via axial histidyl ligation of its (porphinato)zinc moiety even after immobilization on to the solid substrate and subsequent washing.

RESULTS AND DISCUSSION

Computationally designed tetra-α-helical proteins are capable of preferentially binding synthetic, abiological (porphinato)-metal chromophores.[1,3−5] For example, (1) a D_2-symmetric homotetramer bundle capable of binding two (5,15-di[(4-carboxymethyleneoxy)phenyl]porphinato)iron [(DPP)Fe] co-factors,[3] (2) a D_2-symmetric homotetramer bundle capable of binding four (DPP)Fe units,[5] (3) a C_2-symmetric hetero-tetramer bundle capable of binding two light-activatable (DPP)-Zn chromophores,[4] and (4) an asymmetric, single-chain tetrahelical bundle capable of binding two (DPP)Fe species[1] have all been successfully designed and characterized. These designed proteins preferentially bind and target nonbiological cofactors even in the presence of naturally occurring protoporphyrin IX complexes bearing the same metal ion. Likewise, a de novo tetrahelical bundle has been designed that binds both a Ru(bpy)$_2$ (bpy = 2,2′ bipyridyl) unit and a heme cofactor through independent bis-histidine coordination at separate sites, defining an artificial reaction center protein.[45] In sum, this body of work indicates the selectivity in cofactor recognition achievable with carefully designed proteins.

Cofactor Design. **RuPZn** (Chart 1), a chromophore closely related to a structure established to possess an exceedingly large hyperpolarizability at telecommunications-relevant wave-lengths,[13,14,18] was designed and synthesized to facilitate incorporation into a designed protein. The cofactor was synthesized using methods described previously, through cross-coupling a 4′-brominated bis(2,2′;6′,2″-terpyridine)ruthe-nium complex with [5-ethynyl-10,20-bisphenyl-porphinato]-zinc(II). Note that the only difference between **RuPZn** and the parent supermolecule upon which it is based,[13,14,18] lies in the nature of the porphyrin 10- and 20-aryl substituents, which lack bulky 2′,6′-bis(3,3-dimethyl-1-butyloxy) substituents, which were anticipated to be an impediment to the formation of complementary interactions between protein and cofactor. As these 2′,6′-bis(3,3-dimethyl-1-butyloxy) substituents lie orthog-onal to the π-conjugated framework of the chromophore, it was

assumed that this cofactor modification would not impact the *RuPZn* hyperpolarizability relative to the previously established benchmark.

Design of Proteins: *SCRPZ-1*, *SCRPZ-2*, and *SCRPZ-3*. Single-chain, genetically encodable proteins were computationally designed to bind the *RuPZn* cofactor. Previous work has employed synthetic amphiphilic helical bundles comprising multiple peptide chains that bind this class of extended π-electron porphyrin molecules, including *RuPZn*.[23,24,46−48] The amphiphilic nature of the design allows for self-assembly at the air−water interface generating Langmuir monolayers. Our current design, *SCRPZ-1*, differs in that the protein was computationally designed specifically for *RuPZn* and is not simply a promiscuous binder of cofactors containing a (porphinato)zinc moiety. This computational design was done in an attempt to enhance the binding affinity and structural specificity, control the chromophore-localized electrostatic environment, ensure cofactor orientational homogeneity, and produce a more stable material.

The overall construction of the 109-residue protein began with assigning the coordination environment around the (porphinato)zinc moiety (Figure 1). Previous related work involving engineering a (porphinato)zinc (PZn) binding site within a de novo heterotetrameric α-helical bundle provided single histidine coordination for the metalloporphyrin moiety.[4] Presentation of a side-chain conformation of HIS45 consistent with Zn coordination was assisted by the presence on an adjacent helix containing THR8, which is positioned to hydrogen bond to the δ-nitrogen of this histidine.[1,3,4] Design calculations identified a porphyrin-contacting leucine (LEU100) at the "distal" site of the PZn moiety opposite HIS45, in this work and in a previous study (Figure 1).[4]

A suitable tertiary structure was created for binding *RuPZn* (Figure 4). Coordinates of four helices consistent with the cofactor structure and coordination of the central metal ion of the unit were modeled as discussed previously.[1,3,4] Three loops

from an inter-helical loop database were selected and incorporated between helices to generate a single chain backbone as discussed previously for a similar single-chain, four-helix protein.[1]

The model of the tertiary structure containing the *RuPZn* cofactor was used in the computational design of a sequence for the protein. Residues associated with Zn ion coordination (HIS45, THR8) were constrained in their identities and side-chain conformations. The remaining positions were specified using results from a method that self-consistently estimates the site-specific probabilities of amino acids at variable positions in the structure.[1−4,37,49] The method incorporates constraints on sequence properties and uses atomistic energy functions. The resulting designed protein, *SCRPZ-1*, possesses (a) the aforementioned Zn(II) coordinating HIS45, (b) largely hydrophobic residues within its interior near the cofactor that form a cavity that complements the shape of the cofactor, and (c) largely hydrophilic exterior residues (Figure 4). Note that for the *SCRPZ-1* holoprotein, the cofactor constitutes 8% of the total mass (SCRPZ-1 = 12708.5 g/mol, [RuPZn]$^{2+}$ = 1114.2 g/mol, SCRPZ-1 holoprotein = 13822.7).

At micromolar concentrations, *SCRPZ-1* dimerizes in solution, but the monomer is preferred with the addition of isopropanol (vide infra). To arrive at a monomeric form of the protein and probe the robustness of the designed protein's structure and binding properties with respect to exterior mutations, the exterior of the protein was redesigned. Select C_α carbon atoms of the model protein backbone were aligned with the C_α carbon atoms present in a model of the known monomeric protein PA_{SC} (Chart S1).[1] With this structural alignment as a guide, 11 residues were changed to those present at equivalent positions in PA_{SC}. Four additional residues were modified to generate salt bridges with those residues adopted from the PA_{SC} exterior. In addition, four more residues were modified to incorporate two interhelical salt bridges, vide infra. The resulting protein, *SCRPZ-2*, possesses 19 mutations relative to *SCRPZ-1*.

For surface immobilization studies of the protein, four additional C-terminal residues were added to *SCRPZ-1*: GGGC (Figure 4E). The CYS112 residue in the resulting protein, *SCRPZ-3*, provides a reactive residue for covalent attachment to functionalized silica surfaces.

Electronic Absorption Spectroscopy. EAS data of the cofactor in DMSO solvent and the cofactor bound to *SCRPZ-1* and *SCRPZ-2* are presented in Figure 5. As expected, the
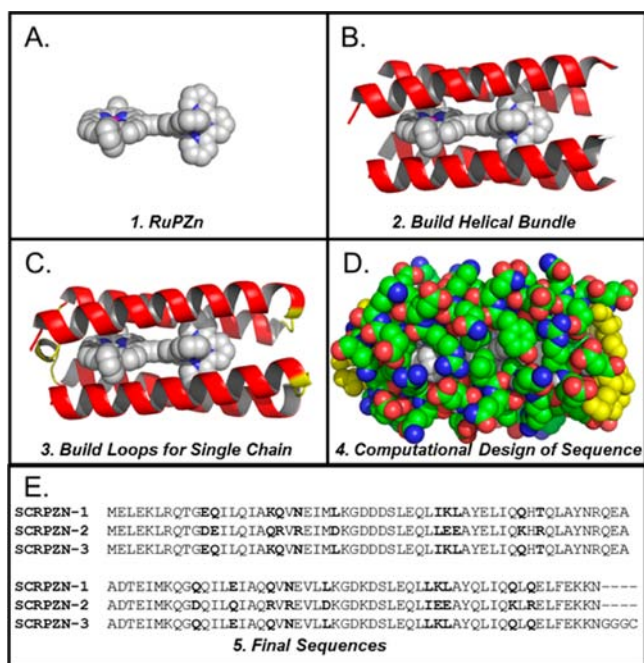

Figure 4. Scheme for design of *SCRPZ-1*, a de novo-designed protein containing the *RuPZn* cofactor.
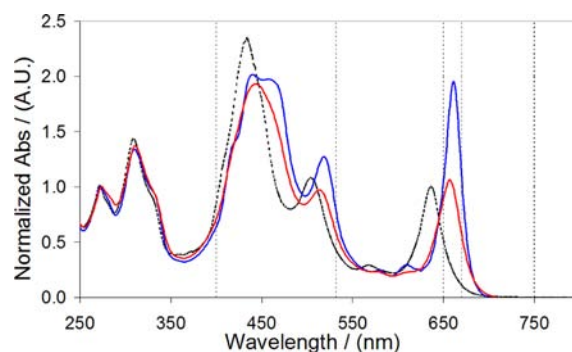

Figure 5. Electronic absorption spectra of *RuPZn* in DMSO solvent (dashed line), holo-*SCRPZ-1* (red line), and holo-*SCRPZ-2* (blue line), normalized at 280 nm. Lines drawn at 400, 532, 650, and 670 nm are included for clarity.

spectrum of the cofactor in DMSO is consistent with that reported previously for the parent supermolecule in acetonitrile solvent.[13] Note that while **RuPZn** exhibits strong mixing of the (porphinato)Zn(II) (PZn)-based oscillator strength with metal polypyridyl charge-resonance bands (as the spectrum does not evince transitions that derive from the simple superposition of precursor compound spectra), spectral qualities are retained that trace their genesis to those of classical PZn and bis(terpyridyl)ruthenium(II) ($[Ru(tpy)_2]^{2+}$) oscillators. **RuPZn** is characterized by (i) a strong ($\varepsilon > 100\,000$ M^{-1} cm^{-1}) absorption near ~435 nm which features significant porphyrin-derived $^1\pi-\pi^*$ Soret (B) band character; (ii) a visible band centered at ~505 nm which exhibits significant $[Ru(tpy)_2]^{2+}$-derived singlet metal-to-ligand charge transfer (^{1}MLCT) character and marked contributions from porphyrin ligand oscillator strength; and (iii) bands localized at ~565 and ~640 nm which exhibit porphyrinic $^1\pi-\pi^*$ Q-state character, with the lower energy, x-polarized transition manifesting features due to symmetry breaking and oscillator strength redistributions that derive from conjugation expansion[8,10,50] and charge resonance character that originates from the ethyne-bridged porphyrin *meso*-carbon-to-terpyridyl-carbon linkage.[13,14] Note as well that the **RuPZn** spectrum exhibits two prominent ultraviolet (UV) absorption bands near 270 and 310 nm that correspond largely to terpyridine localized $\pi-\pi^*$ transitions. While it is recognized that MLCT (d–π^*) and Soret (B)- and Q-band ($\pi-\pi^*$) electronic states mix extensively in these supermolecules,[51] for the sake of simplicity, we utilize these transition labels to denote the dominant contributor to the oscillator strength of a given transition manifold in the discussion that follows.

When bound within the binding site of the de novo-designed proteins, **RuPZn** exhibits spectral features shifted relative to those observed in DMSO solvent (Figure 5). In the **SCRPZ-1** holoprotein, red shifts are observed in the Soret (445 nm), MLCT- (516 nm), and x-polarized Q-band-derived (658 nm) transition manifolds. Similarly, in the **SCRPZ-2** holoprotein, the **RuPZn** spectrum features a red-shifted, clearly split Soret manifold (440 and 459 nm), a red-shifted MLCT-derived transition (520 nm), and a lower energy and intensified Q$_x$-state-derived transition (662 nm). As these **RuPZn** spectral shifts track with protein binding,[1,3–5] these transitions can be used to monitor cofactor–protein association. Note that while the **SCRPZ-1,2** apoproteins feature absorption at 280 nm ($\varepsilon \approx$ 3840 M^{-1} cm^{-1}, due to the $\pi-\pi^*$ transitions of the three Tyr residues), the oscillator strength of this absorbance is virtually negligible relative to that of the chromophore at this wavelength ($\varepsilon > 40\,000$ M^{-1} cm^{-1}).

Spectrophotometric titrations of protein into a solution of **RuPZn** (50 mM phosphate, 150 mM NaCl, pH 7.5 and 1% w/v OG as a surfactant) displayed the expected red-shift in the Q-band upon addition of the proteins (Figure 6). For both proteins, a 1:1 protein:**RuPZn** stoichiometry was observed, with spectral shifts saturating near 1 equiv of the protein added. For **SCRPZ-2**, the equivalence point is not as sharp as it is for **SCRPZ-1**, suggesting a lower binding affinity. Fitting these titration data to a 1:1 equilibrium binding model[52] provides dissociation constants of $K_D = 32 \pm 1$ nM for **SCRPZ-1** and $K_D = 1.23 \pm 0.1$ μM for **SCRPZ-2**. Note that these values represent apparent dissociation constants in the presence the surfactant 1% w/v OG, which was required to enhance the solubility of the cofactor in order to perform the experiments; the cofactor is not soluble in the aqueous buffer alone. These data are
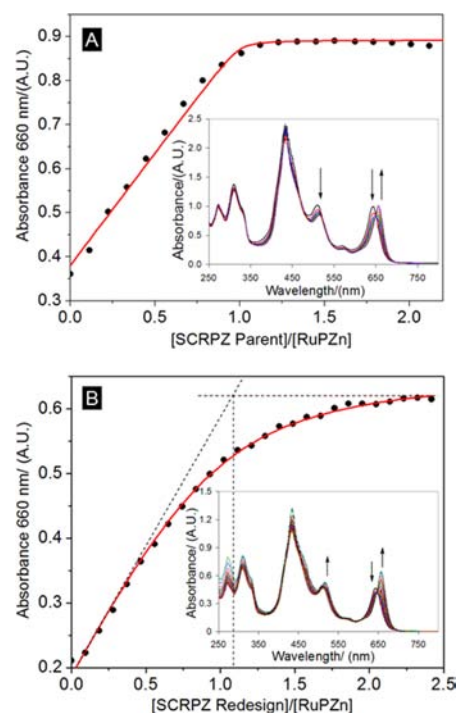

Figure 6. Titrations of protein into a dilute cofactor solution monitored at 660 nm and the corresponding spectra (inset): (A) **SCRPZ-1** and (B) **SCRPZ-2**. Red lines represent fits to a 1:1 equilibrium binding model of protein and cofactor. From these data, K_D(**SCRPZ-1**) = 32 $\pm$ 1 nM and K_D(**SCRPZ-2**) = 1.23 $\pm$ 0.1 μM were determined.

consistent with earlier work that examined a heterotetrameric helical protein that binds two synthetic (porphinato)zinc chromophores ($K_{D,avg} = 0.28$ μM),[4] as well as that which studied **RuPZn** binding to a de novo-designed amphiphilic four-helix bundle peptide in which simple bis(histidyl) ligation was exploited to bind the chromophore ($K_D < 100$ nM).[23] Likewise, other metalloporhyrins established to bind to helical bundle proteins feature experimentally determined cofactor dissociation constants that range from <1 nM to 15 μM.[53] Within our current study, the lower **RuPZn** K_D value obtained for **SCRPZ-1** is not surprising, considering its rigorous computational design; in contrast, the empirical redesign of **SCRPZ-2** appears to have yielded a cofactor pocket that binds **RuPZn** less tightly.

Circular Dichroism Spectroscopy. Circular dichroism (CD) spectra acquired for **SCRPZ-1** and **SCRPZ-2** are consistent with highly helical proteins in both their respective apo and holo forms. The spectra possess minima at 208 and 222 nm with similar mean residue ellipticities, which are indicative of ~60% α-helical content (Figure 7). Both proteins retain these helical signatures in the presence of the cofactor, and the spectral intensities increase slightly for **SCRPZ-1** in the presence of **RuPZn**, but decrease slightly for **SCRPZ-2**. The changes are close to experimental error, and too small to be interpreted in terms of significant changes in secondary structure. On the other hand, in the visible (vis)–near-infrared (NIR) region, the measured ellipticity suggests that the two proteins offer disparate binding environments for the cofactor, exemplified by the observed differences in the CD spectra (Cotton effect) over 400–700 nm spectral domain (Figure 8). Thermal melt profiles of the two systems indicate substantial helical thermostabilities of both the apo and holo forms, as no
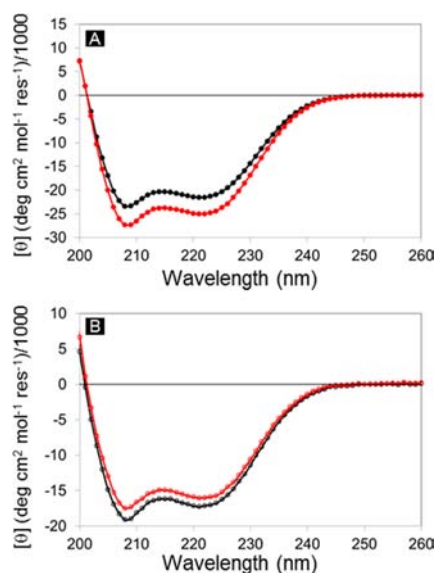
Figure 7. Circular dichroism spectra of (A) *SCRPZ-1* apo (black) and holo (red) and (B) *SCRPZ-2* apo (black) and holo (red).
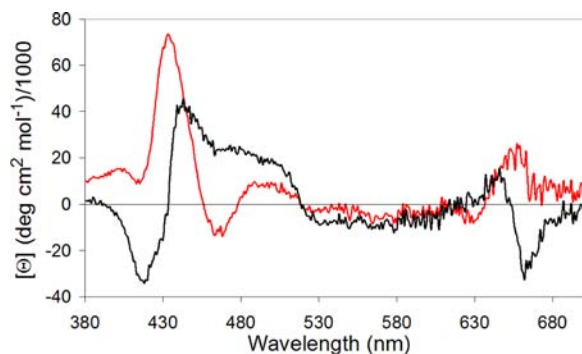

Figure 8. Circular dichroism spectra of the visible region of holo-*SCRPZ-1* (black) and holo-*SCRPZ-2* (red).

cooperative loss of helical content is observed over the temperature range $T = 0-98$ °C (Figure 9).

Size Exclusion Chromatography. Size exclusion chromatography of 20 μM *SCRPZ-1* (50 mM phosphate, 150 mM NaCl, and pH 7.5) indicates a monodisperse, monomeric protein at the expected elution volume, $V_e = 12.5$ mL (Figure
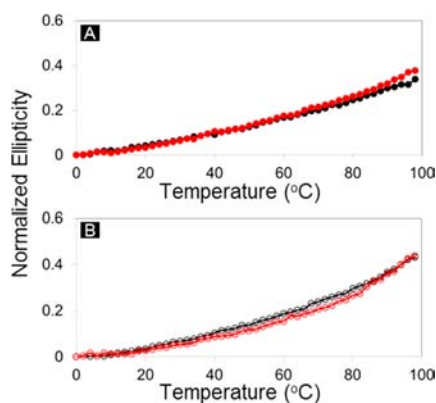

Figure 9. Normalized ellipticity at $\lambda = 222$ nm, $\{[\theta](T) - [\theta](0\,°C)\}/[\theta](0\,°C)$ as a function of temperature: (A) *SCRPZ-1* apo (black) and holo (red); (B) *SCRPZ-2* apo (black) and holo (red).

10A). However, upon addition of the cofactor, higher molecular weight oligomers were observed, with a dimer comprising the
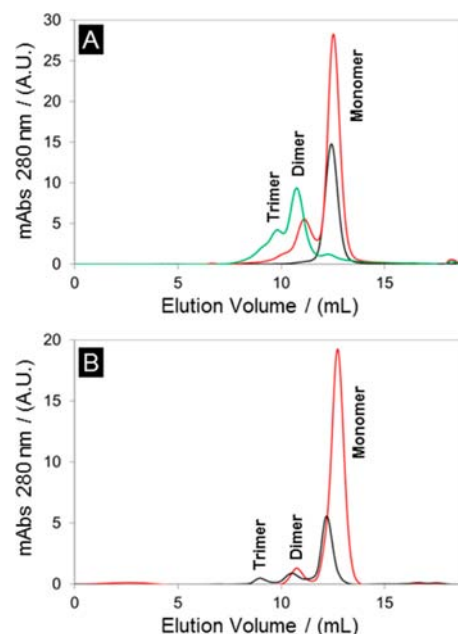

Figure 10. Size exclusion chromatography of (A) *SCRPZ-1* apo (black line), holo (green line), and holo +5 % iPrOH (red line), and (B) *SCRPZ-2* apo (black line) and holo (red line).

dominant species in solution ($V_e = 10.7$ mL). In order to test for oligomerization due to hydrophobic association, the column was treated with 5% isopropanol (v/v), resulting in an equilibrium concentration reflecting ~80% monomer. Collection of this peak, followed by EAS analysis confirmed that the cofactor remained bound to the peptide. In the case of *SCRPZ-2*, the apoprotein eluted as a distribution of monomeric, dimeric, and trimeric species ($V_e = 9.0$, 10.7, and 12.5 mL, respectively; Figure 10B). Upon addition of the cofactor, the holoprotein eluted as ~90% monomer ($V_e = 12.5$ mL). Isopropanol treatment of the column was not necessary to drive the equilibrium toward the monomer state for holo-*SCRPZ-2*.

Analytical Ultracentrifugation: Sedimentation Equilibrium. The oligomerization states of the designed proteins in the apo and holo forms were analyzed via AU. Using a single molecular weight model (assuming a monomeric protein) apo-*SCRPZ-1* (160 μM) yielded an estimated $M_W = 21\,700 \pm 700$ Da. As the expected (calculated) molecular weight is 12 708.5 Da, these data suggest oligomer formation at this concentration (Figure 11). It is noteworthy that this AU-estimated M_W contrasts that determined for apo-*SCRPZ-1* via size exclusion chromatography under similar conditions, which indicated a monodisperse, monomeric protein; in this regard it is important to underscore that the protein concentrations used in these AU studies exceed that utilized for size exclusion chromatography by 10-fold, and likely drives a substantial protein dimer population under these conditions. For holo-*SCRPZ-1* (20 μM), analyzing the data using a single species (assuming a monomeric protein) yielded $M_W = 28\,300 \pm 300$ Da; the corresponding calculated molecular weight is 13 823 Da. Holo-*SCRPZ-1* thus appears to favor a dimeric state under AU experimental conditions, and is consistent with size exclusion chromatographic data (Figure 11).
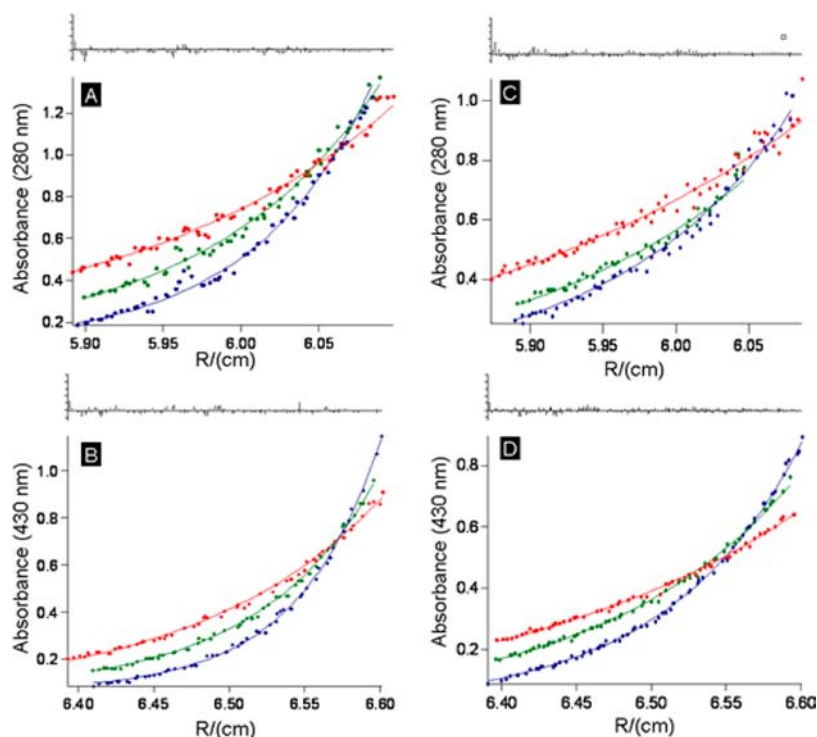
Figure 11. Analytical ultracentrifugation plots (dots) and their respective globally fitted data (solid lines) as monitored at 20, 25, and 30 kRPM (red, green, and blue respectively): (A) apo-**SCRPZ-1**, χ^2 = 3.23; (B) holo-**SCRPZ-1**, χ^2 = 5.40; (C) apo-**SCRPZ-2**, χ^2 = 0.503; and (D) holo-**SCRPZ-2**, χ^2 =2.11.

AU data for **SCRPZ-2** indicate predominant monomeric proteins for both the apo and holo forms. Analysis of the apo-**SCRPZ-2** ([protein] = 160 μM) data using a model that considers only a single species yielded M_W = 13 100 ± 800 Da, consistent with the expected molecular weight of the monomer, 12 942.5 Da. At a concentration of 160 μM, apo-**SCRPZ-2** exists in predominantly the monomeric state. For holo-**SCRPZ-2** (20 μM), AU data analysis using a single component model yields a M_W = 16 500 ± 300 Da, near the expected calculated M_W = 14 057 Da. The slightly higher than expected value is likely due to the presence of a minor dimeric protein population under these AU experimental conditions, resembling the results of the size exclusion chromatographic analysis which indicated that holo-**SCRPZ-2** eluted primarily (~90%) as a monomeric protein.

SCRPZ-1 and **SCRPZ-2** possess the same helical backbone template structure but differ in 19 exterior residues, which alter the oligomerization behavior. In their apo states at concentrations of 20 μM, both **SCRPZ-1** and **SCRPZ-2** proteins exist predominantly in the monomer form, which is consistent with data obtained from size-exclusion chromatography. Upon addition of the **RuPZn** cofactor, **SCRPZ-2** exists predominantly as a monomer, whereas **SCRPZ-1** displays a monomer–dimer–trimer equilibrium. **SCRPZ-1** contrasts **SCRPZ-2** in that it features exterior hydrophobic patches comprising hydrophobic residues in proximity to neutral glutamines. These hydrophobic patches may form points of contact for dimerization, consistent with the observation that treating holo-**SCRPZ-1** with isopropanol increased the population of monomer (Figure 10).

All in all, two proteins have been designed, **SCRPZ-1** and **SCRPZ-2**, that are capable of binding and encapsulating a complex synthetic chromophore, **RuPZn**. The chromophore itself has previously been shown to exhibit an exceptionally high

hyperpolarizability, and an unusual electronically excited triplet state. Critical transient dynamical and nonlinear optical data that characterize the holo-**SCRPZ-1,2** proteins are summarized below.

Excited-State Transient Dynamical Studies. The **RuPZn** chromophoric prototype has previously been studied via pump−probe spectroscopic methods over the femtosecond through microsecond time domains.[13,14,18] Excited-state relaxation dynamics of ethyne-bridged (porphinato)zinc(II)−metal(II)−bis(terpyridyl)ruthenium supermolecules exhibit marked differences from those delineated for their component chromophoric building blocks (PZn and $[\text{Ru(tpy)}_2]^{2+}$). Monomeric (porphinato)zinc(II) compounds generally relax through both the singlet and triplet manifolds, leading to deactivation on both the nanosecond (singlet) and millisecond (triplet) time scales at room temperature.[14,18] Electronically excited $[\text{Ru(tpy)}_2]^{2+}$ undergoes rapid intersystem crossing to the low-lying metal-to-ligand charge transfer (triplet) surface,[54−56] but then is rapidly quenched by thermally populating a low-lying metal-centered (^{3}MC) state such that the ^{3}MLCT lifetime at 298 K is ~250 ps.[57] In **RuPZn** and previously reported related compounds, transient absorption spectra obtained at early time delays (t_{delay} < 400 fs) demonstrate fast excited-state relaxation and the characteristics of a highly polarized T$_1$ excited state; the combined effects of rapid intersystem crossing and strong coupling to low-lying MLCT states gives rise to excited-state lifetimes on the order of tens of microseconds.[14] Interrogation of the electronically excited states of **RuPZn** (data not shown) via pump−probe transient optical methods reveals spectral features characteristic of this class of chromophoric supermolecules that include: (i) prominent visible region bleaching due to ground-state depletion, (ii) a broad, weak transient absorption in the

spectral region between the high oscillator strength ground-state bleaches, and (iii) an expansive, intense $T_1 \rightarrow T_n$ absorption manifold that dominates the 800−1200 nm region of the NIR.[14,18]

Pump−probe spectroscopic studies of holo-**SCRPZ-1** (50 mM phosphate buffer, 5% isopropanol, 150 mM NaCl, pH 7.5) demonstrate transient dynamics and spectral evolution similar to that exhibited by the cofactor in organic solvent. Figure 12
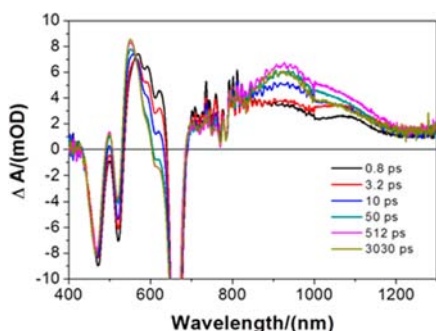

Figure 12. Picosecond time domain magic angle pump−probe transient absorption spectra recorded at several time delays for holo-**SCRPZ-1**. Experimental conditions: ambient temperature, λ_{ex} = 660 nm; solvent, 50 mM phosphate buffer, 5% isopropanol, 150 mM NaCl, pH 7.5.

shows exemplary transient absorption spectral data for holo-**SCRPZ-1** obtained over a 0.7 ps−5.5 ns time domain and highlights the multiexponential nature of its relaxation dynamics. A global exponential fit to these transient absorption data acquired at multiple wavelengths yields three time constants: τ_{rise} = 13.9 ps, τ_{decay} = 1.8 ns, and a long-lived component (τ_{long} > 9.6 ns) that exceeds the track resolution of the instrument. The 13.9 ps component leads to an increase in the intensity of the $T_1 \rightarrow T_n$ NIR transient absorption band; previous studies show that these dynamics are associated with torsional motion about the ethynyl bridge,[18,58−60] with the relaxed ^{3}MLCT state featuring conformeric distributions having a reduced mean torsional angle between the porphyrin and terpyridine least-squares planes. While this relaxed excited triplet state displays augmented $T_1 \rightarrow T_n$ manifold transition oscillator strength with respect to that evident in the initially prepared ^{3}MLCT state of closely related chromophores,[18,59] the oscillator strength evolution observed over time delays ranging from 1 to 50 ps for holo-**SCRPZ-1** is less dramatic than that observed for the chromophore in organic solvent, consistent with a more restricted range of porphyrin−terpyridyl torsional angles for **RuPZn** in the protein matrix relative to solution. Note that **RuPZn** in organic solvent does not manifest a 1.8 ns decay component.

Holo-**SCRPZ-2** (50 mM phosphate buffer, 150 mM NaCl, pH 7.5), which exists predominantly as a monomer in the absence of isopropanol, was interrogated using pump−probe experimental conditions identical to those used for holo-**SCRPZ-1**. Global data fitting shows that holo-**SCRPZ-2** exhibits analogous excited-state relaxation dynamics (τ_{rise} = 12.7 ps, τ_{decay} = 1.8 ns, and τ_{long} > 9.6 ns; Figure 13). The fact that holo-**SCRPZ-2** manifests a 1.8 ns decay component identical to that observed for holo-**SCRPZ-1** in the absence of isopropanol, suggests that this transient decay, that is not observed for **RuPZn** in organic solvent, derives from the anisotropic chromophoric environment provided by the
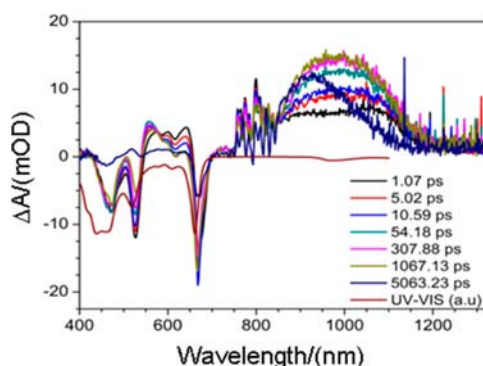

Figure 13. Picosecond time domain magic angle pump−probe transient absorption spectra recorded at several time delays for holo-**SCRPZ-2**. Experimental conditions: ambient temperature, λ_{ex} = 660 nm; solvent, 50 mM phosphate buffer, 150 mM NaCl, pH 7.5. A scaled steady-state absorption spectrum (inverted, red line) is displayed for comparison.

protein. As the fully relaxed **RuPZn** electronically excited triplet features an extensively delocalized T_1-state wave function characterized by substantial charge-separated character,[13,14,18] these observed dynamics are congruent with the expectation that the nature of electronic relaxation for the chromophore within the protein should not necessarily mirror that for **RuPZn** in bulk solvent; in these de novo proteins, the heterogeneous dielectric protein environment gives rise to an excited-state decay channel for unrelaxed **RuPZn** that is not available in homogeneous organic solvent.

Figure 14 displays transient absorption spectral data obtained for holo-**SCRPZ-1** (50 mM phosphate buffer, 5% isopropanol,
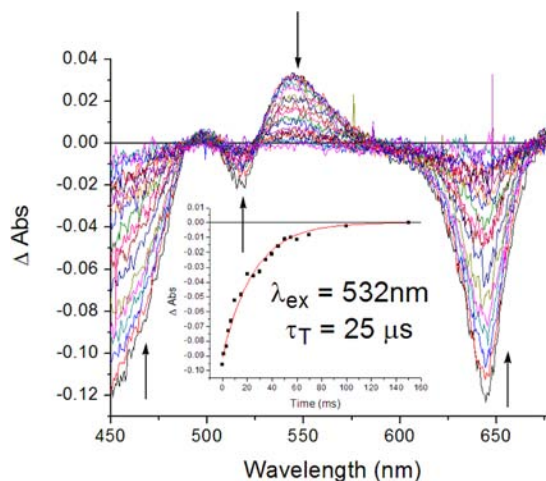

Figure 14. Nanosecond time domain transient absorption spectra obtained for holo-**SCRPZ-1** recorded at multiple time delays. Inset: single exponential decay profile measured at 470 nm (black dots) with the fitted lifetime of 25 μs (solid red line). Experimental conditions: ambient temperature, λ_{ex} = 532 nm; solvent, 50 mM phosphate buffer, 5% isopropanol, 150 mM NaCl, pH 7.5.

150 mM NaCl, pH 7.5) over time delays that range between 1 and 150 μs. Congruent with that observed for **RuPZn** in organic solvent, holo-**SCPZN-1** ground-state bleaching recovery in the B-, MLCT-, and Q-derived spectral domains manifests uniform monoexponential dynamics. Multiwavelength analysis using a single exponential decay model yields a 25 μs triplet lifetime for holo-**SCPZN-1**, comparable to that

determined for *RuPZn* in acetonitrile solvent (44 μs),[13,14,18] indicating that the fully relaxed electronically excited triplet states of *RuPZn* and holo-*SCPZN-1* are similar.

Nonlinear Optical Properties. Dynamic hyperpolarizabilities (β_λ values) were determined from HRS measurements as described previously;[13,40,41] these data are summarized in Table 1. Note that the measured values of β_λ for holo-*SCRPZ-1* and

Table 1. Comparative Dynamic Hyperpolarizabilities Determined for *RuPZn*, holo-*SCPZN-1*, and holo-*SCPZN-2* as a Function Incident Irradiation Wavelength[a]

	β_λ (10^{-30} esu)		
chromophore	800 nm	1300 nm	1340 nm
RuPZn[13]	<50	5100	not measured
holo-*SCRPZ-1*	200 ± 50	1200 ± 200	3100 ± 1000
holo-*SCRPZ-2*	550 ± 150	1000 ± 300	3300 ± 1000

[a]Experimental conditions: for *RuPZn*, acetonitrile solvent, see ref 13; for holo-*SCRPZ-1*, 50 mM phosphate buffer, 5% isopropanol, 150 mM NaCl, pH 7.5; for holo-*SCRPZ-2*, 50 mM phosphate buffer, 150 mM NaCl, pH 7.5.

holo-*SCRPZ-2* are identical within experimental uncertainty, showing that the self-assembly properties of the proteins can effectively be leveraged to construct superstructures of abiological cofactors without affecting the inherent nonlinear optical activity of the bound chromophoric cofactor.

Modest observed differences in the magnitudes of the dynamic hyperpolarizabilities determined for the two de novo proteins and that measured previously for *RuPZn* in acetonitrile solvent derive from the facts that (i) the β_λ spectrum (the irradiation wavelength-dependent magnitude of the hyperpolarizability) depends upon both two- and three-level contributions (transition dipoles between ground and excited states, and transition dipoles among excited states) and (ii) B-, Q-, and MLCT-derived transition manifolds contribute to the measured hyperpolarizability.[13,25] Theory demonstrates convincingly that the measured magnitudes of the hyperpolarizabilities near 800 and 1300 nm for *RuPZn* are sensitive to the transition energies and oscillator strengths of the B-, Q-, and MLCT-derived transition manifolds.[25] Because holo-*SCRPZ-1* and holo-*SCRPZ-2* exhibit spectral shifts relative to the *RuPZn* benchmark (note particularly that for the Q-derived states near 650 nm, Figure 5), it is thus not surprising that variations in the wavelength-dependent nonlinear response are observed, and that small shifts in laser irradiation wavelength near 1300 nm give rise to substantial differences in the measured dynamic hyperpolarizability (Table 1).

These data show that the designed proteins *SCRPZ-1* and *SCRPZ-2* are capable of binding and orienting *RuPZn*, while preserving critical nonlinear optical (e.g., a large hyperpolarizability at long wavelength) and photophysical (e.g., a microsecond time scale triplet-state lifetime) properties of the supermolecular chromophore. *SCRPZ-1* and *SCRPZ-2* thus define functional scaffolds that disperse the cofactor in an aqueous environment and protect the chromophore from detrimental aggregation effects. The protein also provides a means to immobilize the material on a substrate and enable engineering of novel self-assembly motifs.

Self-Assembled Monolayers of SCRPZ-3 Covalently Attached to Solid Substrates. Using standard protocols, the C-terminus of the *SCRPZ-1* protein was functionalized with a thiol linker, -GGGC, which is denoted as *SCRPZ-3*. Like

SCRPZ-1, *SCRPZ-3* specifically binds *RuPZn*; holo-*SCRPZ-3* manifests spectral characteristics identical to those of holo-*SCRPZ-1*. Monolayers of holo-*SCRPZ-3* were immobilized on a self-assembled monolayer of 3-aminopropyldimethylethoxysilane via conjugation between the amino functional group and the thiol of the C-terminal cysteine of *SCRPZ-3* using SMCC conjugation. The linear EAS of the self-assembled holoprotein monolayer on fused silica resembled that of holo-*SCRPZ-1* (Figure 5), and not of the *RuPZn* chromophore in organic solvent, consistent with the fact that *RuPZn* remained bound to the single-chain protein, even after immobilization of the complex on the surface of the solid substrate and subsequent washing.

XR from the covalently attached self-assembled monolayers of holo-*SCRPZ-3* on GeSi multilayer substrates allowed determination of the electron density profile of the monolayer, where interferometry was employed to phase the reflectivity data (Figure 15). The derived profile is consistent with the long axis of the four-helix bundle lying parallel to the plane of the monolayer. This observed orientation for these tetra-α-helical bundle proteins may result from the inherent flexibilities of (a) the covalent linkage between the C-terminus of the peptide and the substrate surface and (b) the GGGC terminal sequence. Though the proteins can be affixed to the substrate at high surface densities, their orientational order contrasts with that realized for amphiphilic helical bundles that bind related abiological porphyrin-based chromophores,[23,24,46−48] where the amphiphilic nature of the design provided a perpendicular orientation in Langmuir monolayers at the air−water interface at high surface pressures. However, these oligomeric, amphilic bundles were not tailored to particular cofactors and possessed an excess of histidine residues (four) over what is necessary to bind a single chromophore/four-helix bundle via axial ligation of the PZn moiety. By comparison, holo-*SCRPZ-3* is a robust protein that provides not only more precise control of the local cofactor environment but also the dispersion and processing of RuPZn in buffer solution and its immobilization at solid interfaces.

■ CONCLUSION

This work reports the first example of a single-chain protein computationally designed to possess four α-helical segments and fold to encapsulate with high specificity an abiological chromophore that exhibits exceptional nonlinear optical (NLO) properties. The single-chain 109-residue tetra-α-helical bundle, *SCRPZ-1*, binds and disperses an insoluble hyperpolarizable chromophore, ruthenium(II) [5-(4′-ethynyl-(2,2′;6′,2″-terpyridinyl))-10,20-bis(phenyl)porphinato]zinc-(II)-(2,2′;6′,2″-terpyridine)$^{2+}$ (*RuPZn*), in aqueous buffer solution at a 1:1 stoichiometry. Characterization data are consistent with a thermostable, highly helical protein having a secondary structure congruent with the model tertiary structure used to design the sequence. While *SCRPZ-1* retains its helical content in the presence of the cofactor, holo-*SCRPZ-1* readily dimerizes; an empirical redesign of the protein exterior produced a stable monomeric protein, *SCRPZ-2*, that also displayed a 1:1 protein:cofactor stoichiometry.

For holo-*SCRPZ-1* and holo-*SCRPZ-2* in aqueous buffer, the encapsulated cofactor evinces photophysical properties resembling those exhibited by the *RuPZn* cofactor in dilute organic solvent: femtosecond, nanosecond, and microsecond time scale pump−probe transient absorption spectroscopic data reveal intensely absorbing holoprotein excited states having large
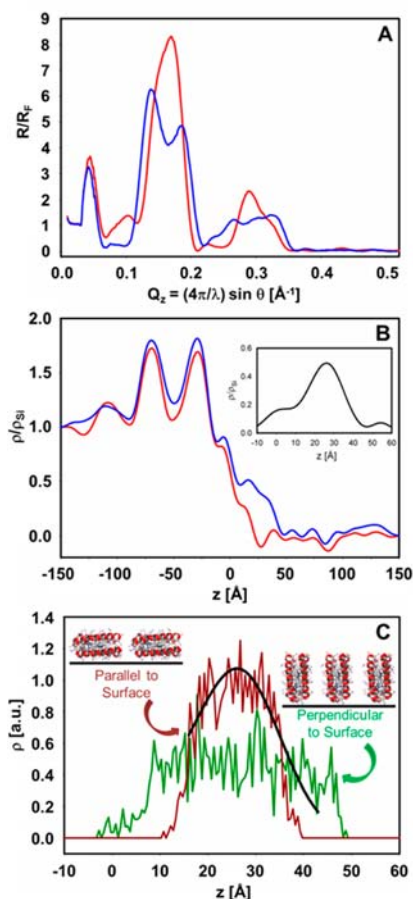
Figure 15. (A) Fresnel-normalized X-ray reflectivity from the alkylated GeSi multilayer substrate reacted with the linker and washed (red) versus that for the same substrate with covalently attached holo-***SCRPZ-3*** (blue) following washing. (B) Electron density profiles, derived from the normalized reflectivity data via interferometry employing the GeSi multilayer as the reference structure, where the red and blue designations are those from (A). The two maxima from the Ge features in the GeSi multilayer appear for $z < 0$ Å, while the features of the moist helium atmosphere appear for $z > 50$ Å in these profiles, with the wavelength of the latter fluctuations indicative of the spatial resolution and their amplitude of the noise level in the derived profiles. The inset shows the difference electron density profile due to holo-***SCRPZ-3*** that occurs within 10 Å $< z < 50$ Å. This feature appears as a single electron density maximum whose fwhm is ~25 Å. (C) Calculated electron density profiles for the design target structure for holo-***SCRPZ-3***, assuming that the long axis of the four-helix bundle is either parallel (brown) or perpendicular (green) to the plane of the self-assembled monolayer. The former is consistent with the experimentally determined profile for holo-***SCRPZ-3*** within these self-assembled monolayers.

spectral bandwidth that penetrate deep in the NIR energy regime. The holo-***SCRPZ-1*** and holo-***SCRPZ-2*** electronically excited triplet states exhibit microsecond time scale lifetimes characteristic of the ***RuPZn*** chromophore. HRS measurements carried out at an incident irradiation wavelength (λ_{inc}) of 1340 nm for these proteins demonstrate an exceptional dynamic hyperpolarizabilty ($\beta_{1340} = 3100 \times 10^{-30}$ esu). Modification of the C-terminus of the protein with a GGGC extension yields a variant, ***SCRPZ-3***; X-ray reflexivity and linear spectroscopy establish that holo-***SCRPZ-3*** can be immobilized on an alkylamine-modified silicon surface in a densely packed fashion without loss of the cofactor. Given that proteins bind and

control the conformation and orientation of cofactors, modulate their functional properties, and can encode for protein−protein organization over mesoscopic and macroscopic length scales, appropriately de novo-designed proteins that bind high-performance abiological chromophores promise new opportunities to control bulk-phase acentric order of nonlinear optical functional elements and yield bioinspired nanostructures and soft-matter materials having unique electro-optic functionality.

■ ASSOCIATED CONTENT

Ⓢ Supporting Information

Sequence alignment of PA$_{sc}$ and SCRPZ-1, backbone alignment of PA$_{sc}$ and SCRPZ-1, mapping of the acidic and basic residues in space-filling models, gene sequences for protein expression, and synthetic details. This material is available free of charge via the Internet at http://pubs.acs.org.

■ AUTHOR INFORMATION

Corresponding Authors
bill.degrado@ucsf.edu
saven@sas.upenn.edu
michael.therien@duke.edu

Present Address
¶A.L.: Fox Chase Cancer Center, Philadelphia, PA 19111-2434

Notes
The authors declare no competing financial interest.

■ ACKNOWLEDGMENTS

■ REFERENCES

(1) Bender, G. M.; Lehmann, A.; Zou, H.; Cheng, H.; Fry, H. C.; Engel, D.; Therien, M. J.; Blasie, J. K.; Roder, H.; Saven, J. G.; DeGrado, W. F. *J. Am. Chem. Soc.* **2007**, *129*, 10732.
(2) Calhoun, J. R.; Kono, H.; Lahr, S.; Wang, W.; DeGrado, W. F.; Saven, J. G. *J. Mol. Biol.* **2003**, *334*, 1101.
(3) Cochran, F. V.; Wu, S. P.; Wang, W.; Nanda, V.; Saven, J. G.; Therien, M. J.; DeGrado, W. F. *J. Am. Chem. Soc.* **2005**, *127*, 1346.
(4) Fry, H. C.; Lehmann, A.; Saven, J. G.; DeGrado, W. F.; Therien, M. J. *J. Am. Chem. Soc.* **2010**, *132*, 3997.
(5) McAllister, K. A.; Zou, H. L.; Cochran, F. V.; Bender, G. M.; Senes, A.; Fry, H. C.; Nanda, V.; Keenan, P. A.; Lear, J. D.; Saven, J. G.; Therien, M. J.; Blasie, J. K.; DeGrado, W. F. *J. Am. Chem. Soc.* **2008**, *130*, 11921.
(6) Meyers, F.; Marder, S. R.; Pierce, B. M.; Bredas, J. L. *J. Am. Chem. Soc.* **1994**, *116*, 10703.
(7) Marder, S. R.; Cheng, L. T.; Tiemann, B. G.; Friedli, A. C.; Blancharddesce, M.; Perry, J. W.; Skindhoj, J. *Science* **1994**, *263*, 511.
(8) LeCours, S. M.; Guan, H. W.; DiMagno, S. G.; Wang, C. H.; Therien, M. J. *J. Am. Chem. Soc.* **1996**, *118*, 1497.
(9) LeCours, S. M.; DiMagno, S. G.; Therien, M. J. *J. Am. Chem. Soc.* **1996**, *118*, 11854.
(10) Priyadarshy, S.; Therien, M. J.; Beratan, D. N. *J. Am. Chem. Soc.* **1996**, *118*, 1504.

(11) Karki, L.; Vance, F. W.; Hupp, J. T.; LeCours, S. M.; Therien, M. J. *J. Am. Chem. Soc.* **1998**, *120*, 2606.

(12) Anderson, H. L. *Chem. Commun.* **1999**, 2323.

(13) Uyeda, H. T.; Zhao, Y. X.; Wostyn, K.; Asselberghs, I.; Clays, K.; Persoons, A.; Therien, M. J. *J. Am. Chem. Soc.* **2002**, *124*, 13806.

(14) Duncan, T. V.; Rubtsov, I. V.; Uyeda, H. T.; Therien, M. J. *J. Am. Chem. Soc.* **2004**, *126*, 9474.

(15) Kang, H.; Facchetti, A.; Zhu, P. W.; Jiang, H.; Yang, Y.; Cariati, E.; Righetto, S.; Ugo, R.; Zuccaccia, C.; Macchioni, A.; Stern, C. L.; Liu, Z. F.; Ho, S. T.; Marks, T. J. *Angew. Chem., Int. Ed.* **2005**, *44*, 7922.

(16) Zhang, T. G.; Zhao, Y. X.; Asselberghs, I.; Persoons, A.; Clays, K.; Therien, M. J. *J. Am. Chem. Soc.* **2005**, *127*, 9710.

(17) Zhang, T. G.; Zhao, Y. X.; Song, K.; Asselberghs, I.; Persoons, A.; Clays, K.; Therien, M. J. *Inorg. Chem.* **2006**, *45*, 9703.

(18) Duncan, T. V.; Ishizuka, T.; Therien, M. J. *J. Am. Chem. Soc.* **2007**, *129*, 9691.

(19) Duncan, T. V.; Song, K.; Hung, S. T.; Miloradovic, I.; Nayak, A.; Persoons, A.; Verbiest, T.; Therien, M. J.; Clays, K. *Angew. Chem., Int. Ed.* **2008**, *47*, 2978.

(20) Keinan, S.; Therien, M. J.; Beratan, D. N.; Yang, W. T. *J. Phys. Chem. A* **2008**, *112*, 12203.

(21) Reeve, J. E.; Collins, H. A.; De Mey, K.; Kohl, M. M.; Thorley, K. J.; Paulsen, O.; Clays, K.; Anderson, H. L. *J. Am. Chem. Soc.* **2009**, *131*, 2758.

(22) Therien, M. J. *Nature* **2009**, *458*, 716.

(23) Xu, T.; Wu, S. P.; Miloradovic, I.; Therien, M. J.; Blasie, J. K. *Nano Lett.* **2006**, *6*, 2387.

(24) Strzalka, J.; Xu, T.; Tronin, A.; Wu, S. P.; Miloradovic, I.; Kuzmenko, I.; Gog, T.; Therien, M. J.; Blasie, J. K. *Nano Lett.* **2006**, *6*, 2395.

(25) Hu, X.; Xiao, D.; Keinan, S.; Asselberghs, I.; Therien, M. J.; Clays, K.; Yang, W.; Beratan, D. N. *J. Phys. Chem. C* **2010**, *114*, 2349.

(26) Ishizuka, T.; Sinks, L. E.; Song, K.; Hung, S. T.; Nayak, A.; Clays, K.; Therien, M. J. *J. Am. Chem. Soc.* **2011**, *133*, 2884.

(27) Dalton, L. R.; Harper, A. W.; Robinson, B. H. *Proc. Natl. Acad. Sci. U.S.A.* **1997**, *94*, 4842.

(28) Dalton, L. R.; Steier, W. H.; Robinson, B. H.; Zhang, C.; Ren, A.; Garner, S.; Chen, A. T.; Londergan, T.; Irwin, L.; Carlson, B.; Fifield, L.; Phelan, G.; Kincaid, C.; Amend, J.; Jen, A. *J. Mater. Chem.* **1999**, *9*, 1905.

(29) Robinson, B. H.; Dalton, L. R.; Harper, A. W.; Ren, A.; Wang, F.; Zhang, C.; Todorova, G.; Lee, M.; Aniszfeld, R.; Garner, S.; Chen, A.; Steier, W. H.; Houbrecht, S.; Persoons, A.; Ledoux, I.; Zyss, J.; Jen, A. K. Y. *Chem. Phys.* **1999**, *245*, 35.

(30) Steier, W. H.; Chen, A.; Lee, S. S.; Garner, S.; Zhang, H.; Chuyanov, V.; Dalton, L. R.; Wang, F.; Ren, A. S.; Zhang, C.; Todorova, G.; Harper, A.; Fetterman, H. R.; Chen, D. T.; Udupa, A.; Bhattacharya, D.; Tsap, B. *Chem. Phys.* **1999**, *245*, 487.

(31) Liakatas, I.; Cai, C.; Bosch, M.; Jager, M.; Bosshard, C.; Gunter, P.; Zhang, C.; Dalton, L. R. *Appl. Phys. Lett.* **2000**, *76*, 1368.

(32) Ma, H.; Liu, S.; Luo, J. D.; Suresh, S.; Liu, L.; Kang, S. H.; Haller, M.; Sassa, T.; Dalton, L. R.; Jen, A. K. Y. *Adv. Funct. Mater.* **2002**, *12*, 565.

(33) Dalton, L. *Polym. Photon. Appl. I* **2002**, *158*, 1.

(34) Luo, J. D.; Haller, M.; Ma, H.; Liu, S.; Kim, T. D.; Tian, Y. Q.; Chen, B. Q.; Jang, S. H.; Dalton, L. R.; Jen, A. K. Y. *J. Phys. Chem. B* **2004**, *108*, 8523.

(35) Brooks, B. R.; Bruccoleri, R. E.; Olafson, B. D.; States, D. J.; Swaminathan, S.; Karplus, M. *J. Comput. Chem.* **1983**, *4*, 187.

(36) Laskowski, R. A.; Macarthur, M. W.; Moss, D. S.; Thornton, J. M. *J. Appl. Crystallogr.* **1993**, *26*, 283.

(37) Kono, H.; Saven, J. G. *J. Mol. Biol.* **2001**, *306*, 607.

(38) Lahr, S. J.; Engel, D. E.; Stayrook, S. E.; Maglio, O.; North, B.; Geremia, S.; Lombardi, A.; DeGrado, W. F. *J. Mol. Biol.* **2005**, *346*, 1441.

(39) Papp, A.; Vanderkooi, J. M.; Owen, C. S.; Holtom, G. R.; Phillips, C. M. *Biophys. J.* **1990**, *58*, 177.

(40) Olbrechts, G.; Strobbe, R.; Clays, K.; Persoons, A. *Rev. Sci. Instrum.* **1998**, *69*, 2233.

(41) Olbrechts, G.; Wostyn, K.; Clays, K.; Persoons, A. *Opt. Lett.* **1999**, *24*, 403.

(42) Blasie, J. K.; Zheng, S.; Strzalka, J. *Phys. Rev. B* **2003**, *67*, 224201.

(43) Krishnan, V.; Strzalka, J.; Liu, J.; Liu, C. A.; Kuzmenko, I.; Gog, T.; Blasie, J. K. *Phys. Rev. E* **2010**, *81*, 021604.

(44) Kneller, L. R.; Edwards, A. M.; Nordgren, C. E.; Blasie, J. K.; Berk, N. F.; Krueger, S.; Majkrzak, C. F. *Biophys. J.* **2001**, *80*, 2248.

(45) Cristian, L.; Piotrowiak, P.; Farid, R. S. *J. Am. Chem. Soc.* **2003**, *125*, 11814.

(46) Gonella, G.; Dai, H.-L.; Fry, H. C.; Therien, M. J.; Krishnan, V.; Tronin, A.; Blasie, J. K. *J. Am. Chem. Soc.* **2010**, *132*, 9693.

(47) Krishnan, V.; Tronin, A.; Strzalka, J.; Fry, H. C.; Therien, M. J.; Blasie, J. K. *J. Am. Chem. Soc.* **2010**, *132*, 11083.

(48) Koo, J.; Park, J.; Tronin, A.; Zhang, R.; Krishnan, V.; Strzalka, J.; Kuzmenko, I.; Fry, H. C.; Therien, M. J.; Blasie, J. K. *Langmuir* **2012**, *28*, 3227.

(49) Slovic, A. M.; Kono, H.; Lear, J. D.; Saven, J. G.; DeGrado, W. F. *Proc. Natl. Acad. Sci. U.S.A.* **2004**, *101*, 1828.

(50) LeCours, S. M.; Philips, C. M.; de Paula, J. C.; Therien, M. J. *J. Am. Chem. Soc.* **1997**, *119*, 12578.

(51) Lin, V. S.-Y.; DiMagno, S. G.; Therien, M. J. *Science* **1994**, *264*, 1105.

(52) Petros, A. K.; Reddi, A. R.; Kennedy, M. L.; Hyslop, A. G.; Gibney, B. R. *Inorg. Chem.* **2006**, *45*, 9941.

(53) Reedy, C. J.; Gibney, B. R. *Chem. Rev.* **2004**, *104*, 617.

(54) McCusker, J. K. *Acc. Chem. Res.* **2003**, *36*, 876.

(55) Damrauer, N. H.; Weldon, B. T.; McCusker, J. K. *J. Phys. Chem. A* **1998**, *102*, 3382.

(56) Damrauer, N. H.; Cerullo, G.; Yeh, A.; Boussie, T. R.; Shank, C. V.; McCusker, J. K. *Science* **1997**, *275*, 54.

(57) Winkler, J. R.; Sutin, N. *Inorg. Chem.* **1987**, *26*, 220.

(58) Rubtsov, I. V.; Susumu, K.; Rubtsov, G. I.; Therien, M. J. *J. Am. Chem. Soc.* **2003**, *125*, 2687.

(59) Angiolillo, P. J.; Uyeda, H. T.; Duncan, T. V.; Therien, M. J. *J. Phys. Chem. B* **2004**, *108*, 11893.

(60) Kumble, R.; Palese, S.; Lin, V. S.-Y.; Therien, M. J.; Hochstrasser, R. M. *J. Am. Chem. Soc.* **1998**, *120*, 11489.